Cancer Letters 452 (2019) 203–212

Contents lists available at ScienceDirect

Cancer Letters

journal homepage: www.elsevier.com/locate/canlet

Original Articles

MicroRNA-365a-3p inhibits c-Rel-mediated NF-κB signaling and the progression of pancreatic cancer

Libo Yin[a], Xi Xiao[a], Christina Georgikou[a], Yefeng Yin[a], Li Liu[a], Svetlana Karakhanova[a], Yiqiao Luo[a], Jury Gladkich[a], Joerg Fellenberg[b], Carsten Sticht[c], Norbert Gretz[c], Wolfgang Gross[a], Ingrid Herr[a,*]

[a] Molecular OncoSurgery, Section Surgical Research, Department of General, Visceral & Transplant Surgery, University of Heidelberg, Heidelberg, Germany
[b] Research Centre for Experimental Orthopedics, Clinic for Orthopedics and Trauma Surgery, University of Heidelberg, Germany
[c] Medical Research Centre, Medical Faculty Mannheim, University of Heidelberg, Germany

ARTICLE INFO

Keywords:
Pancreatic cancer
Sulforaphane
NF-κB signaling
microRNA

ABSTRACT

NF-κB contributes to the aggressiveness of pancreatic ductal adenocarcinoma (PDA), which is counteracted by the bioactive agent sulforaphane. We investigated sulforaphane-induced microRNA signaling and its influence on progression features. Using established cell lines, microRNA and gene arrays, we predicted miR-365a as the top candidate for the sulforaphane-induced inhibition of the NF-κB subunit c-Rel. The lipofection of miR-365a-3p mimics inhibited the luciferase activity of a c-Rel 3′-UTR construct, as well as c-Rel expression, NF-κB activity, and tumor viability, migration, and clonogenicity, whereas apoptosis was induced. *In vivo*, miR-365a-3p reduced the volume of tumor xenografts and the expression of progression markers. In a tissue array, the expression of miR-365a-3p was absent in almost all 91 malignant tissues but not in 5 normal tissues, thus confirming the previous results. Our observations suggest that sulforaphane-induced miR-365a-3p expression inhibits NF-κB activity by downregulating c-Rel, which prevents the progression of PDA.

1. Introduction

Pancreatic ductal adenocarcinoma (PDA) is one of the most lethal malignancies with poor therapeutic options [1]. Complete surgical resection is the only way of curing this cancer, but late diagnosis limits surgical treatment. PDA is notoriously resistant to treatment, and only a few patients benefit from chemotherapy [2].

A major reason for chemotherapy resistance is the almost constantly activated NF-κB signaling pathway [3]. NF-κB complexes consist of proteins present in the cytoplasm, namely, p50, p52, RelA/p65, RelB and cRel [4,5]. We demonstrated that broccoli-derived isothiocyanate sulforaphane inhibits NF-κB signaling in PDA by inhibiting the transactivation activity of the potent NF-κB subunit c-Rel [6]. Patients with high c-Rel levels exhibit shorter progression-free survival than patients with lower c-Rel levels, according to the Human Protein Atlas Databank (https://www.proteinatlas.org/ENSG00000162924REL/pathology/tissue/pancreatic+cancer#ihc).

MicroRNAs (miRNAs) are small, approximately 22-nucleotide (nt)-long RNAs [7]. More than one-third of all human genes might be regulated by miRNAs [8]. The dysregulation of miRNA often leads to tumorigenesis and tumor progression, followed by migration and invasion. Depending on the type of miRNA and the cellular context, both anti-oncogenic and pro-oncogenic effects were observed [9].

This study investigated whether sulforaphane-induced miRNAs may be involved in the regulation of NF-κB activity and consequently the progression of PDA. We treated PDA cells with sulforaphane and performed a miRNA gene array, followed by bioinformatics analysis. miR-365a-3p was identified as the top candidate for c-Rel regulation. This assumption was verified by *in vitro*, *in vivo* and patient tissue studies, and the results demonstrated that the loss of miR-365a-3p expression was correlated with the progression features of PDA, whereas sulforaphane activated miR-365a-3p expression and reversed malignancy.

Abbreviations: Cancer stem cells, CSCs; Pancreatic ductal adenocarcinoma, PDA; Chorioallantoic membrane, CAM; Intraductal papillary mucinous neoplasm, IPMN

* Corresponding author. Section Surgical Research, Im Neuenheimer Feld 365, 69120, Heidelberg, Germany.
E-mail addresses: Yin@uni-heidelberg.de (L. Yin), xiaoxidaidai@outlook.com (X. Xiao), georgikou@uni-heidelberg.de (C. Georgikou), yefeng541009@gmail.com (Y. Yin), l.liu@uni-heidelberg.de (L. Liu), karakhanova@uni-heidelberg.de (S. Karakhanova), Luo@uni-heidelberg.de (Y. Luo), gladkich@uni-heidelberg.de (J. Gladkich), carsten.sticht@medma.uni-heidelberg.de (C. Sticht), Norbert.Gretz@medma.uni-heidelberg.de (N. Gretz), WGross@uni-hd.de (W. Gross), i.herr@uni-heidelberg.de (I. Herr).

https://doi.org/10.1016/j.canlet.2019.03.025
Received 16 November 2018; Received in revised form 19 March 2019; Accepted 19 March 2019

2. Methods

2.1. Tumor cell lines

The established human PDA cell lines AsPC-1, BxPC-3, PANC-1, and MIA-PaCa2 were purchased from the American Type Culture Collection (ATCC, Manassas, VA, USA) and cultured as described [10].

2.2. Patient tissue

A paraffin-embedded pancreatic cancer tissue array was obtained from BioCat GmbH (Heidelberg, Germany/US Biomax, Inc., Rockville, Maryland, USA).

2.3. Reagents

Sulforaphane (≥95%) (Sigma-Aldrich, St. Louis, MO, USA) was prepared in DMSO as a 100 mM stock solution and stored in aliquots at −20 °C. Each aliquot was used only once immediately after thawing. The final concentrations of the solvents in media were 0.1% or less.

2.4. Xenotransplantation of pancreatic cancer cells to fertilized chicken eggs

Briefly, fertilized eggs from genetically identical hybrid Lohman Brown (LB) chickens were obtained from a local ecological hatchery (Geflügelzucht Hockenberger, Eppingen, Germany). The treated cells were seeded onto chorioallantoic membranes (CAMs) on day 9 of chick embryo development. On day 18, the tumors were resected, followed by tumor xenotransplantation, and the treatment evaluation of tumor take, tumor growth and metastasis was performed as described previously [11].

2.5. Cell viability

PDA cells were resuspended at a final concentration of $4 \times 10^4 \sim 10^5$/ml and plated onto 96-well microplates at 100 µl per well. After treatment, the cell viability was examined by MTT assay as described [12].

2.6. Colony-forming assay

Twenty-four hours after lipofection, the cells were seeded and analyzed as described.

2.7. Wound healing assay

Twenty-four hours after lipofection, the cells were treated and analyzed as described [10].

2.8. Western blot analyses

Western blot analyses were performed as described [6]. Rabbit polyclonal Abs against Bcl-2 (#2876, 1:1000) and c-Rel (#4727, 1:1000) were both purchased from Cell Signaling (Danvers, USA), and a mouse monoclonal Ab against β-actin (A1978, 1:5000) was purchased from Sigma-Aldrich (St. Louis, USA). All primary antibodies were incubated at 4 °C overnight.

2.9. Immunohistochemical and immunofluorescence staining

Staining was performed on frozen tissue sections or in established cell lines as previously described [13]. Rabbit polyclonal Abs against c-Rel (#4727, 1:100; Cell Signaling, Danvers, USA) or CXCR4 (ab124824, 1:200; Abcam, Cambridge, UK) and the rabbit monoclonal Ab anti-c-Met (ab74217, 1:100; Abcam) were used and incubated at 4 °C overnight.

2.10. mRNA and miRNA profiling

The GeneChip™ Human Gene 2.0 ST Array (Thermo Fisher Scientific Inc., Carlsbad, USA) and the GeneChip™ miRNA 4.0 Array (Thermo Fisher) was used for mRNA and miRNA profiling, respectively.

2.11. In silico analysis

Putative miRNAs predicted to target the 3′-UTR of cRel (Gene ID: ENSG00000162924) were validated by the miRWalk database (http://zmf.umm.uni-heidelberg.de/apps/zmf/mirwalk2/) using a minimum interaction seed length of 6 base pairs ($P < 0.05$). From this analysis, a list of miRNAs targeting c-Rel was made and compared to known sulforaphane-induced miRNAs whose -log10 P was higher than 1.5, resulting in a joint list of miRNAs of sulforaphane-induced miRNAs targeting c-Rel. The primary target sequences between the seed sequence of miR-365a-3p and its counterpart within the REL 3′-untranslated region (3′-UTR) were then identified with the TargetScan database (http://www.targetscan.org/vert_72/).

2.12. MicroRNA transfection

MirVana™ mimics and nonsense miRNAs (mock) (Thermo Fisher Scientific Inc., Dreieich, Germany) at 50 nM each were transfected into the cells using Lipofectamine 2000 (Thermo Fisher Scientific Inc.) with a reverse transfection method as described in the manufacturer's instructions. The following sequences were used: hsa-let-7c: ugaggua-guagguuguaugguu, hsa-miR-550a-5p: agugccugagggaguaagagccc, hsa-miR-125a-5p: ucccugagacccuuuaaccuguga, and hsa-miR-365a-3p: uaaugccccuaaaaauccuuau.

2.13. Dual-Luciferase® reporter assay

The following vectors were used: the pMirTarget luciferase vector carrying the full-length human REL 3′-UTR (pMirTarget_REL_3′-UTR_firefly, 543 bp), the pMirTarget empty vector (both from OriGene, Rockville, USA) and pGL4.73_hRluc/SV40 as an endogenous control (Promega, Mannheim, Germany). The transfection and detection procedures were performed as previously described [14].

2.14. miRNA and mRNA extraction and RT-qPCR

The RNeasy® Mini Kit and miRNeasy® Mini Kit (Qiagen, Qiagen, Hilden, Germany) were used for the isolation of cell line-derived mRNA and miRNA. TaqMan® Small RNA Assays and TaqMan® Gene Expression Assays (Thermo Fisher, Darmstadt, Germany) were used for RT-qPCR according to the manufacturer's instructions.

2.15. Electrophoretic mobility shift assay (EMSA)

The NucBuster™ Protein Extraction Kit (Merck, Darmstadt, Germany) was used for the isolation of nuclear extracts, from which 5 µg was incubated with a master mix (2 µL 10 × binding buffer, 1 µL Poly (dI•dC), 2 µL 25 mM DTT, and 1 µL IRDye 700-conjugated to NF-κB oligonucleotide, adjusted to 20 µL with water) (LI-COR® Biosciences, Lincoln, USA) for 30 min at room temperature in the dark. The NF-κB double-strand oligonucleotide sequences were 5′-AGA GAT TGC CTG ACG TCA GAG AGC TAG C-3′ and 3′-TCA ACT CCC CTG AAA GGG TCC G-5'. After incubation, 1 µL of 10 × Orange Loading Dye (LI-COR® Biosciences, Lincoln, USA) was added, and the DNA–protein complexes were separated on a native 4% polyacrylamide gel. The gel was run at 100 V for approximately 45 min in 1 × TBE buffer. Finally, the gel was exposed by the Odyssey® CLx Infrared Imaging System (LI-COR® Biosciences, Lincoln, USA).

2.16. Detection of apoptosis and necrosis by FACS analysis

Briefly, 5×10^5 cells were collected at 24 h after lipofection by trypsinization and stained with phycoerythrin (PE)-conjugated Annexin V and 7AAD (BD Biosciences, Heidelberg, Germany) according to the manufacturer's instructions. The number of apoptotic cells was determined using a flow cytometer (BD Biosciences, New Jersey, USA).

2.17. Detection of miR-365a-3p expression by in situ hybridization

The miRCURY LNA™ microRNA Detection Kit (Qiagen, Hilden, Germany) was used according to the manufacturer's instructions [15] to stain paraffin-embedded pancreatic cancer tissue. The hybridization was performed for 2 h at 53 °C using digoxigenin-labeled LNA probes for miR-365a-3p: 5′ATAAGGATTTTTAGGGGCATTA3′, or a scrambled miRNA as a negative control (Qiagen). After stringent washes, the bound LNA probes were detected with an alkaline phosphatase-conjugated digoxigenin antibody and NBT/BCIP as a substrate. The sections were mounted using Roti-Mount FluorCare (Roth, Karlsruhe, Germany).

2.18. Statistical analyses

The data obtained with established cell lines are presented as the means ± SD from at least three separate experiments, which were performed at least in triplicate. The significance of the data was analyzed using Student's t-test for parametric data and the Mann–Whitney test for nonparametric data. The Pearson product-moment correlation was performed to measure the linear correlation between two variables X and Y. For the immunohistochemistry or immunofluorescence experiments, the expression intensity and percentage of positive cells were determined by counting the number of differentiated cells in 10 fields of view for each group. $P < 0.05$ was considered statistically significant. $^*P < 0.05$, $^{**}P < 0.01$.

3. Results

3.1. Sulforaphane enhances the expression of miR-365a-3p

To detect the sulforaphane-induced differential regulation of miRNAs, we harvested RNA from untreated or sulforaphane-treated AsPC-1 cells and performed miRNA microarray expression profiling. Based on the bioinformatics evaluation, we identified several significantly ($P < 0.05$) differentially regulated miRNAs, which are presented as a volcano plot (Fig. 1A), by which changes in large data sets can be quickly identified. The x-axis shows the fold change of down- or upregulated miRNAs, and the y-axis shows the level of significance. The top downregulated miRNA was miR-27b-5p, and the top upregulated miRNA was miR-4497. To identify the most NF-κB-relevant miRNAs, we analyzed the results *in silico* with the miRWalk database. We identified 666 miRNA candidates predicted to target the NF-κB transactivation competent subunit c-Rel and 162 miRNA candidates related to sulforaphane (Fig. 1B, Table S1). The two groups of candidates were matched, resulting in 50 miRNA candidates predicted to target c-Rel and be induced by sulforaphane. These 50 miR candidates were further limited by the selection criteria to be (1) upregulated by sulforaphane and (2) relevant for tumorigenesis and cancer progression. The results are shown in a heat map (Fig. 1C). Finally, let-7c-5p, miR-550a-5p, miR125a-5p and miR-365a-3p were selected as the most relevant, and the regulation of these miRNAs by sulforaphane was analyzed by RT-qPCR in AsPC-1 cells. However, unlike the microarray results, miR-550a-5p was downregulated, and the expression of miR125a-5p and let-7c-5p was not significant (Fig. 1D). The only miRNA expression pattern we could confirm was that of miR-365a-3p, which was strongly and significantly upregulated at 24 h after sulforaphane treatment. The upregulation of miR-365a-3p was confirmed in PANC-1, MIA-PaCa-2 and BxPC-3 cells and a strong and significant upregulation was found in the BxPC-3 cell line (Fig. 1E). Therefore, miR-365a-3p was selected as the most relevant miRNA candidate. To further highlight the importance of miR-365a-3p signaling in c-Rel regulation, we performed a mRNA profiling array with the RNA of untreated and sulforaphane-treated AsPC-1 cells and analyzed the results by a gene family clustering analysis using the KEGG (Kyoto Encyclopedia of Genes and Genomes) search tool [16]. We identified NF-κB as one of the 12 most significantly regulated pathways ($P < 0.01$) (Fig. 1F), and a heat map of the KEGG results demonstrates that sulforaphane treatment indeed induced the significant downregulation of c-Rel expression. In addition to c-Rel, 93 other NF-κB-related genes and NF-κB subunits were differentially regulated upon sulforaphane treatment (Table S2).

3.2. miR-365a-3p inhibits c-rel expression by binding to its 3′-UTR

Because sulforaphane inhibits c-Rel binding activity [6] and PDA patients with enhanced c-Rel levels exhibited shorter progression-free survival (https://www.proteinatlas.org/ENSG00000162924REL/pathology/tissue/pancreatic+cancer#ihc), we investigated the correlation between miR-365a-3p and c-Rel expression. BxPC-3 and AsPC-1 cells were lipofected with miR-365a-3p mimics or a mock control mimic, and the levels of miR-365a-3p were examined by qRT-PCR. Compared to the control, the expression of miR-365a-3p was strongly and significantly increased (Fig. 2A), suggesting successful overexpression by lipofection. Next, we predicted the biological targets of miR-365a-3p and its seed regions in target mRNAs by using the TargetScan online database [17]. This analysis resulted in the identification of three putative miR-365a-3p binding sites in the 3′-UTR region of c-Rel (Fig. 2B). To evaluate the regulation of c-Rel by miR-365a-3p, we lipofected a commercially available luciferase reporter construct expressing the c-Rel 3′-UTR (Fig. S1) into BxPC-3 cells and cotransfected a firefly reporter construct or a Renilla control plasmid together with either the miR-365a-3p mimic or a mock mimic control. Twenty-four hours after transfection, the luciferase activity was quantified in a luminescence microplate reader. We observed the significantly reduced luciferase activity of the c-Rel reporter upon cotransfection of miR-365a-3p, which was not observed with the controls (Fig. 2C). Next, we determined whether the overexpression of miR-365a-3p might be able to regulate the expression of c-Rel. Therefore, we analyzed the expression of c-Rel mRNA and protein in BxPC-3 and AsPC-1 cells after lipofection with miR-365a-3p mimics or mock mimics. In miR-365a-3p-transfected cells, the expression of c-Rel was more than 30% lower than that in control cells, as evaluated by qPCR (Fig. 2D). Similarly, the c-Rel protein expression level was lower in miR-365a-3p-transfected cells than in control cells, as assessed by western blot analysis, followed by an evaluation of the pixel identities of the bands by ImageJ (Fig. 2E). Immunofluorescence analysis confirmed that the expression of c-Rel was downregulated in miR-365a-3p-overexpressing BxPc-3 and AsPC-1 cells (Fig. 2F).

3.3. miR-365a-3p induces apoptosis and inhibits progression features

Our previous results suggested that NF-κB mediates apoptosis resistance and tumor progression in PDA cells mainly by its c-Rel subunit [6]. Therefore, we wanted to examine whether the overexpression of miR-365a-3p, and thus the inhibition of c-Rel expression, would affect NF-κB DNA binding activity with subsequent reversion of apoptosis resistance and tumor progression features. Using miR-365a-3p-overexpressing BxPC-3 and AsPC-1 cells and the respective controls, we evaluated the DNA binding activity by electrophoretic mobility shift assay (EMSA). Nuclear extracts of the cells were harvested at 24 h after lipofection with miR-365a-3p and a mock mimic control and incubated with IRDye700 infrared-conjugated oligonucleotides carrying the consensus NF-κB binding site. In control reactions, the nuclear extracts were incubated without oligonucleotide or with a 100-fold excess of

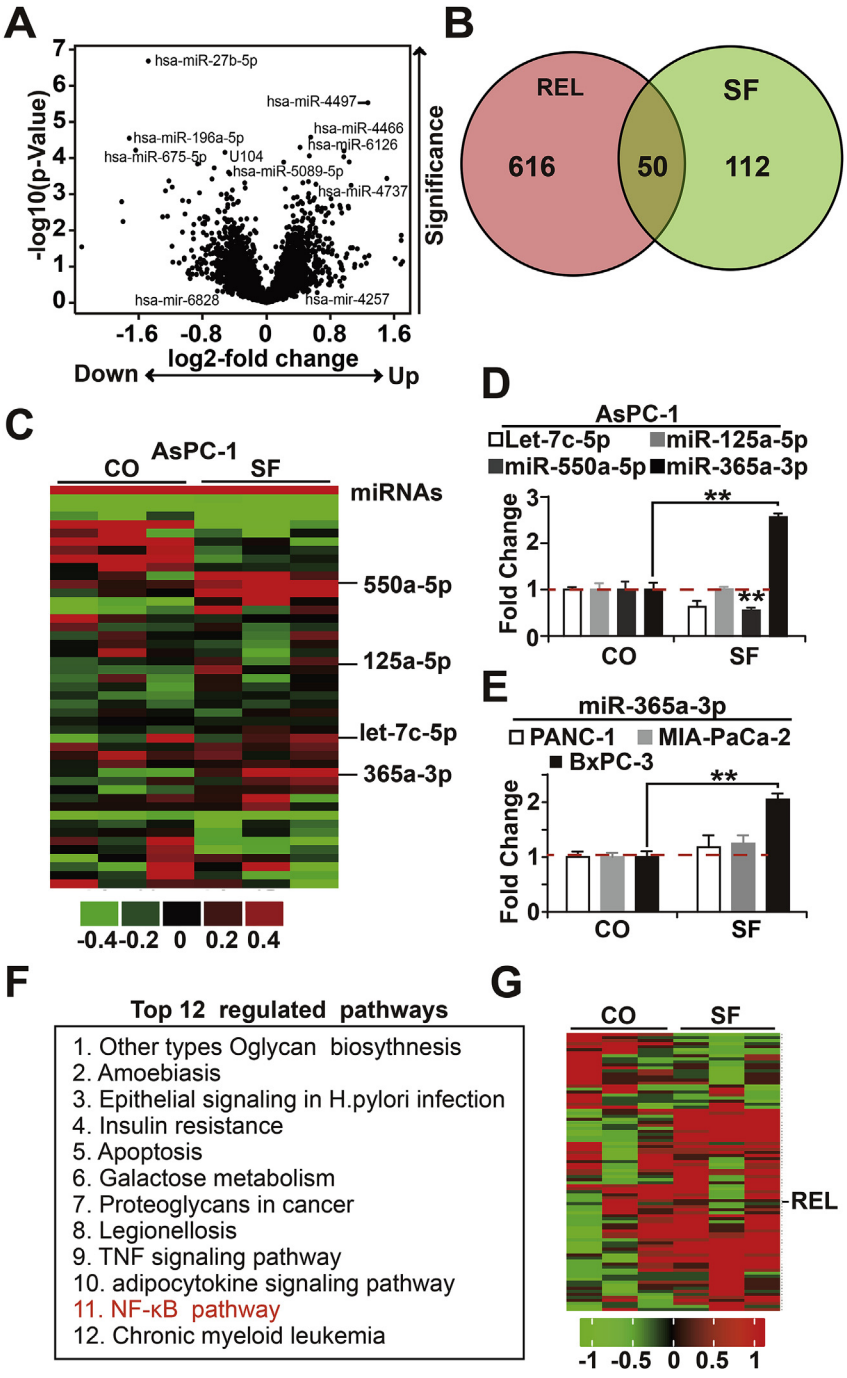

Fig. 1. Sulforaphane upregulates miR-365a-3p. AsPC-1 cells were left untreated (CO) or were treated with 10 nM sulforaphane (SF) for 24 h, followed by RNA isolation. miRNA array analysis and bioinformatics evaluation were performed to select the most significantly dysregulated miRNAs related to the following key words: sulforaphane and c-Rel. (A) The volcano plot shows the miRNA distribution. On the y-axis, the *P*-values and significance were plotted. On the x-axis, the fold change is represented. (B) Venn diagram showing differentially expressed miRNAs. The 666 putative miRNAs targeting c-Rel are indicated in green, while the top 162 sulforaphane-induced miRNAs (-log10 P > 1.5) are indicated in red. The overlapping region indicated that sulforaphane induced 50 miRNAs targeting c-Rel. (C) The heat map presented 50 differentially expressed microRNAs targeting c-Rel. The red colors indicate high expression, and the green colors indicate low expression within a scale from 0.4 to −0.4. (D) The miRNA microarray data were validated by RT-qPCR to confirm the 4 most relevant miRNA candidates, let-7c-5p, miR-550a-5p, miR125a-5p, and miR-365a-3p. AsPC-1 cells were treated as mentioned in A, followed by RT-qPCR analysis. The dotted, red line marks the expression levels of controls. (E) Pancreatic cancer cells were treated as described above, and the relative expression of miR-365a-3p was also detected in the pancreatic cancer cell lines PANC-1, MIA-PaCa2, and BxPC-3. The fold change was normalized to the mock control. (F) The mRNA was harvested from AsPC-1 cells and treated as described in A, followed by gene expression profiling in triplicate. The mRNA expression profiling is listed in the top 12 regulated pathways (**$P < 0.01$). (G) A heat map of mRNA candidates was created, which showed changes in the expression of NF-κB-related genes in the untreated group (CO) and sulforaphane-treated group (SF), where red indicates fold changes of increased transcript expression and blue indicates the downregulation of genes within a scale from −1 to 1. (For interpretation of the references to color in this figure legend, the reader is referred to the Web version of this article.)

nonlabeled NF-κB oligonucleotide. The expected DNA/protein binding complexes were separated by gel electrophoresis from the unbound, free oligonucleotides, and the bands were visualized with a LI-COR® imaging system. Three strong NF-κB complexes were visible in the mock control bands, which were weaker in miR-365a-3p-overexpressing cells and absent in the negative and competitive controls, as expected (Fig. 3A). Next, we examined the expression of the anti-apoptotic c-Rel/p50 target protein Bcl-2 [18] by western blot analysis, which demonstrated the downregulation of Bcl-2 in miR-365a-3p-overexpressing BxPC-3 and AsPC-1 cells (Fig. 3B). In addition, apoptosis was evaluated by staining the cells with Annexin V/7AAD. As expected, the lipofection of miR-365a-3p led to a minor increase in the percentage of apoptotic cells in both cell lines because the inhibition of NF-κB activity alone without additional stimulus does not induce strong apoptosis (Fig. S2). Next, we accessed whether the activation of miR-365a-3p would affect cancer progression features and examined the viability of miR-365a-3p-overexpressing BxPC-3 and AsPC-1 cells. Compared to the mock controls, miR-365a-3p overexpression reduced the viability significantly in both cell lines (Fig. 3D). Similarly, the clonogenicity (Fig. 3E) and the wound healing capacity were significantly reduced (Fig. 3F).

3.4. miR-365a-3p inhibits tumor growth in an in vivo xenograft egg model

After establishing the functional effects of miR-365a-5p *in vitro*, we performed xenograft studies. The chicken egg is a naturally immunodeficient system that does not reject foreign tissue and supports the growth of xenograft tumors by host blood vessels and stroma [19], similar to immunodeficient mice. Lipofected BxPC-3 cells were transplanted to the chorioallantoic membrane (CAM) on day 9 of chick

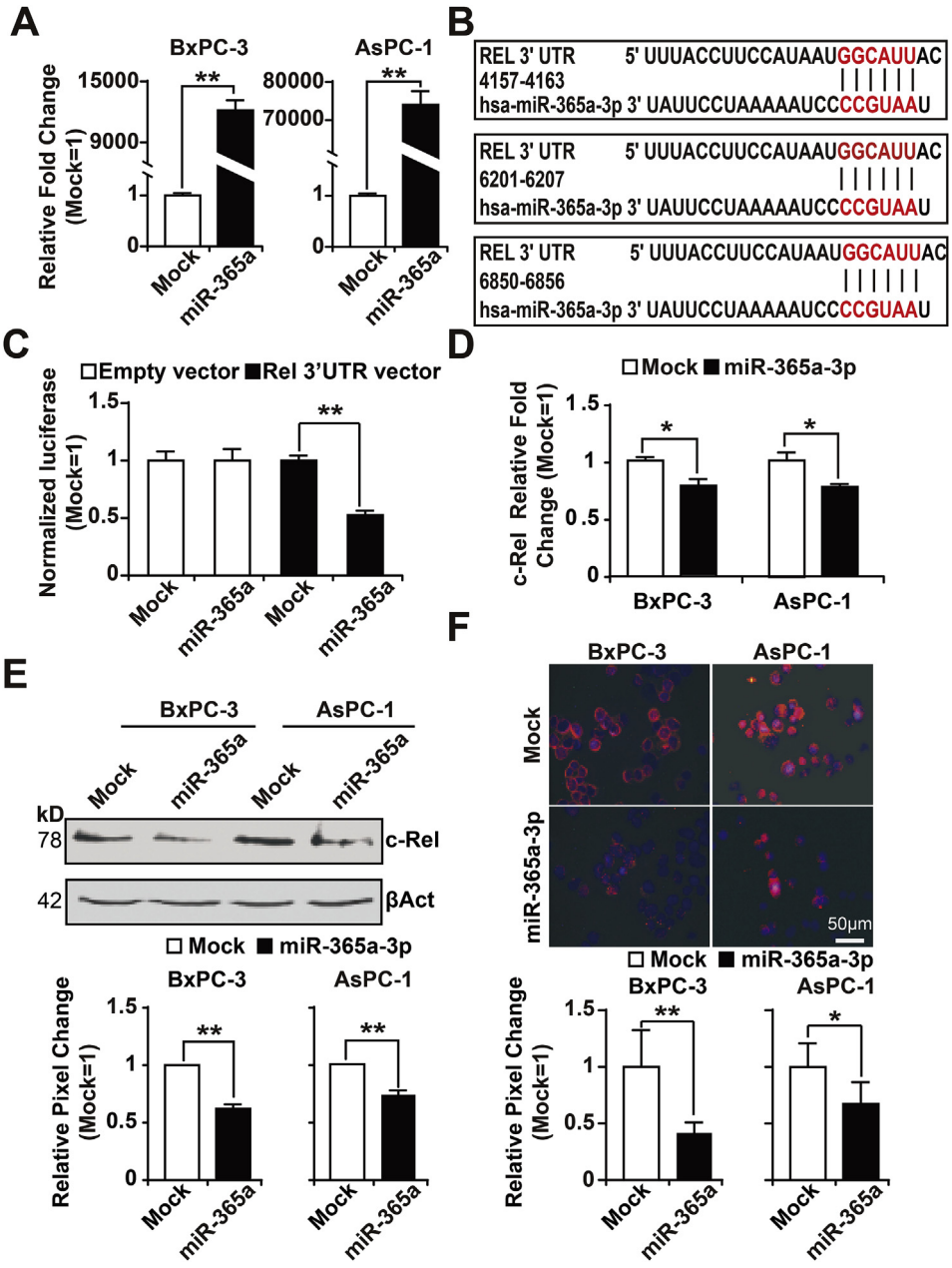

Fig. 2. miR-365a-3p directly targets the REL 3′-UTR. (A) BxPC-3 and AsPC-1 cells were transfected with miR-365a-3p mimic (miR-365a-3p) or nonsense miRNAs (mock). Twenty-four hours later, miR-365a-3p expression was analyzed by qPCR. (B) The three putative sites for the binding of miR-365a-3p to the REL 3′-UTR were identified using the TargetScan database. The seed-binding regions are marked in red. (C) BxPC-3 cells were cotransfected with a firefly reporter construct of the REL 3′-UTR plasmid in the presence or absence of either 50 nM miR-365a-3p mimic or mock. The co-transfection of a Renilla luciferase (0.25 ng/μl) served as a control for equal conditions. Twenty-four hours after transfection, the expression of Renilla and firefly luciferase was detected. Firefly luciferase activities were normalized to Renilla luciferase activities. (D) The cells were treated as described in point A, and quantitative RT-qPCR analysis was performed to detect c-Rel mRNA expression in BxPC-3 and AsPC-1 cells. (E) Representative western blot showing c-Rel protein expression. β-actin served as an internal reference for equal conditions. The pixel intensities of bands of three independent experiments were determined with ImageJ. We normalized in each of 3 individual experiments the different values on the respective MOCK control value, which means that the dominator is different for each experiment. The relative pixel changes are shown below. (F) Subsequently, immunofluorescence staining was performed for c-Rel detection. (For interpretation of the references to color in this figure legend, the reader is referred to the Web version of this article.)

development. At that time point, the blood vessel system of the embryo was dense enough to support tumor growth. The tumors were resected on day 18. Genomic DNA was harvested from some of the tumors in each group, and the levels of miR-365a-3p were measured by qPCR. The findings revealed that the levels of miR-365a-3p were still 6-fold higher at 9 days after xenotransplantation than those in control cells transfected with a mock control only (Fig. 5A). Accordingly, the mean tumor sizes of xenografts with high miR-365a-3p expression were significantly decreased, as measured by calipers (Fig. 4B). To obtain knowledge on c-Rel expression in xenograft tissues, we examined the expression of c-Rel by immunofluorescence staining, which resulted in a specific, red signal in mock control cells that was lower in miR-365a-3p-lipofected xenografts (Fig. 4C upper panel). For quantification, we measured the intensity of the c-Rel-specific red fluorescence by ImageJ in 10 different tumor sections per group and calculated the mean fluorescence intensities. This analysis confirmed lower c-Rel expression levels in miR-365a-3p-overexpressing tumors (Fig. 4C lower panel). The high levels of miR-365a-3p were correlated with a higher percentage of apoptosis, as concluded from the staining of the active fragment of the apoptosis marker caspase-3 by immunohistochemistry and quantitative analysis (Fig. 4D). Similarly, the expression of progression markers, such as the cancer stem cell marker c-Met or the metastasis and invasion marker CXCR4, was significantly decreased (Fig. 4E).

3.5. Loss of miR-365a-3p expression correlates with the malignancy of PDA patient tissue

To further highlight the importance of our results for patients, we used a pancreas cancer tissue array with 91 human pancreatic cancer tissues and 5 normal pancreatic tissues, including information on TNM, clinical stage and pathology grade (Fig. S3). We evaluated the levels of miR-365a-3p by *in situ* hybridization (Fig. 5A and B), followed by quantification of the signals by scoring the staining intensity in 10 vision fields. The malignant tissues on average expressed less miR-365a-3p than did normal tissues. We confirmed a negative correlation between pathological grading and miR-365a- 3p expression ($P < 0.0001$, Pearson's correlation coefficient = −0.4309) (Fig. 5D).

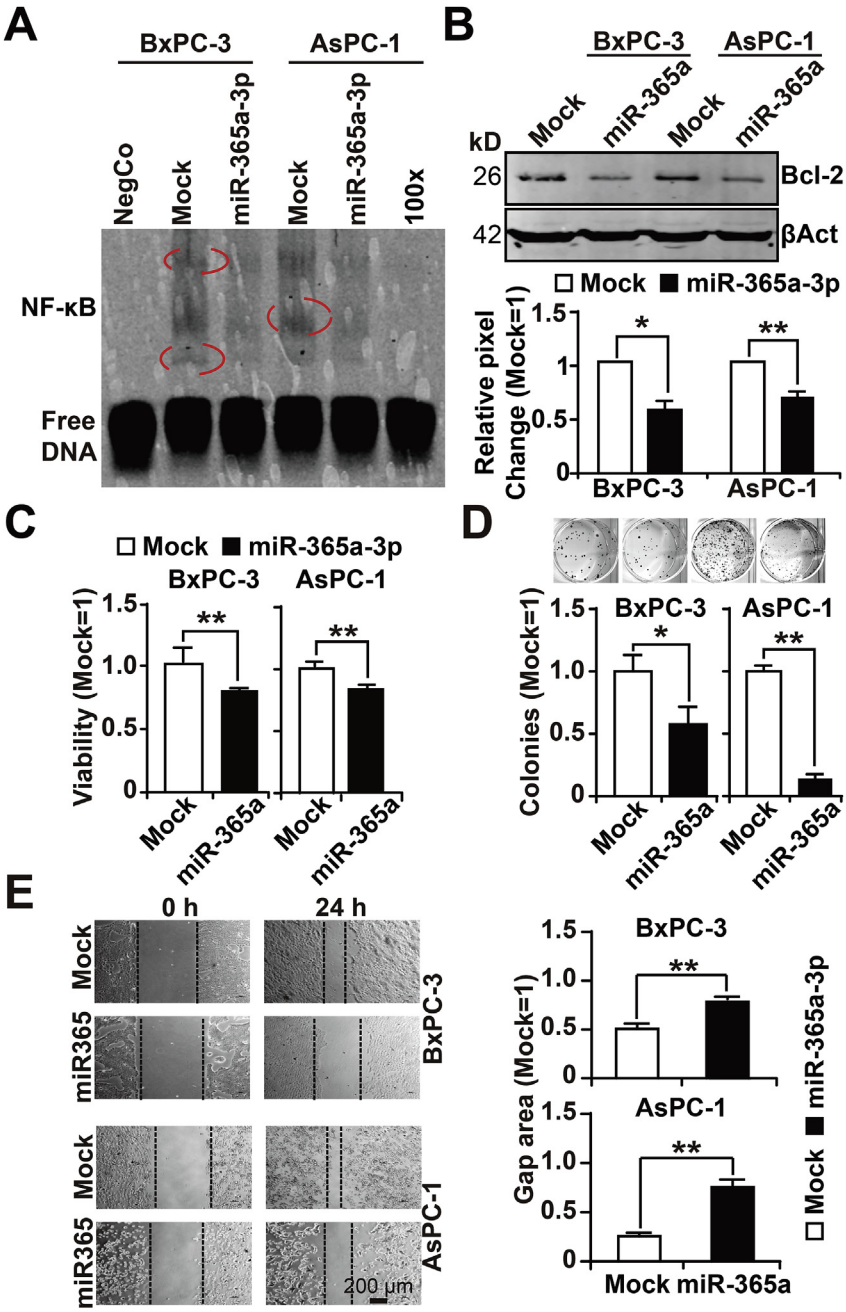

Fig. 3. miR-365a-3p inhibits NF-κB binding activity and progression features (A) Nuclear proteins were extracted from pancreatic cancer cell lines at 24 h after the lipofection of miR365a-3p or mock control mimics and incubated with an IRDye700-conjugated oligonucleotide of the NF-κB consensus binding site, followed by electrophoretic mobility shift assay (EMSA). For the negative control, the IRDye700-conjugated NF-κB oligonucleotide was incubated without nuclear extract (NegCO). For the competition control, a 100-fold excess (100 ×) of a nonconjugated NF-κB consensus sequence was added to the bandshift reaction. After electrophoresis, the shifts were evaluated on a LI-COR® infrared imaging system. (B) The expression of Bcl-2 was determined by western blot analysis in BxPC-3 and AsPC-3 cells (upper panel), and the pixel intensity of the bands was quantified and is shown in the diagram (lower panel). (C) Similarly, the cellular viability was measured by MTT assay. (D) Transfected cells were plated at low density (500 BxPC-3 or 1000 AsPC-1 cells/well) onto 6-well plates. After two weeks, colonies containing more than 50 cells were evaluated under a microscope. The plating efficiency as a percent was calculated as (number of colonies/number of seeded cells) × 100. (E) Twenty-4 h after transfection, the cells were trypsinized and seeded at high density onto 12-well plates. After an additional 24 h, when the cells reached approximately 90% confluence, a scratch was made in the middle of the cell layer by using a yellow pipette tip. Photographs of the wounded region were obtained immediately at 0 h and at 24 h after scratching by microscopy at 100 × magnification. The size of the gap area was analyzed with ImageJ software. . (For interpretation of the references to color in this figure legend, the reader is referred to the Web version of this article.)

4. Discussion

In the present study, we analyzed whether the bioactive agent sulforaphane may normalize enhanced NF-κB activity in PDA cells by inducing miRNA signaling. Using miRNA and gene microarray analysis, followed by bioinformatics and *in vivo* and *in silico* evaluation, we identified miR-365a-3p as the most relevant sulforaphane-regulated miRNA candidate for the inhibition of c-Rel expression.

Our findings are in agreement with the epigenetic regulation of tumor growth by diverse miRNAs in many different tumor entities, where the dysregulation of miRNA signaling was related to various human cancers [20]. The upregulation of our top candidate miR-365a-3p was observed in human lung adenocarcinoma tissue compared to the adjacent matched normal cancerous tissue [21] and in the serum of patients suffering from cystic fibrosis-associated liver disease [22]. Previous results in lung cancer are in contrast with our results in PDA. In our model, higher levels of miR-365a-3p correlated with cancer progression. We do not know the reason for the obviously conflicting data, but these findings emphasize the known complexity and often tissue-specific signaling of miRNAs, as an individual miRNA can target multiple genes, and each gene can be regulated by several miRNAs [23].

The bioinformatics analysis of our miRNA and RNA microarray results and the use of several online databases identified miR-365a-3p as the most important candidate for the regulation of the NF-κB subunit c-Rel. Indeed, we were able to confirm by luciferase assays that miR-365a-3p diminishes c-Rel expression by binding to its 3′-UTR region, suggesting that the observed reduced levels of miR-365a-3p are involved in the c-Rel-driven progression of PDA. Accordingly, the well-known contribution of c-Rel to the malignant progression of solid tumors [24–30] supports our conclusion. In this regard, our search in THE HUMAN PROTEIN ATLAS (https://www.proteinatlas.org/ENSG00000162924-REL/pathology/tissue/pancreatic+cancer) revealed that PDA patients with low cRel expression (n = 114) survive

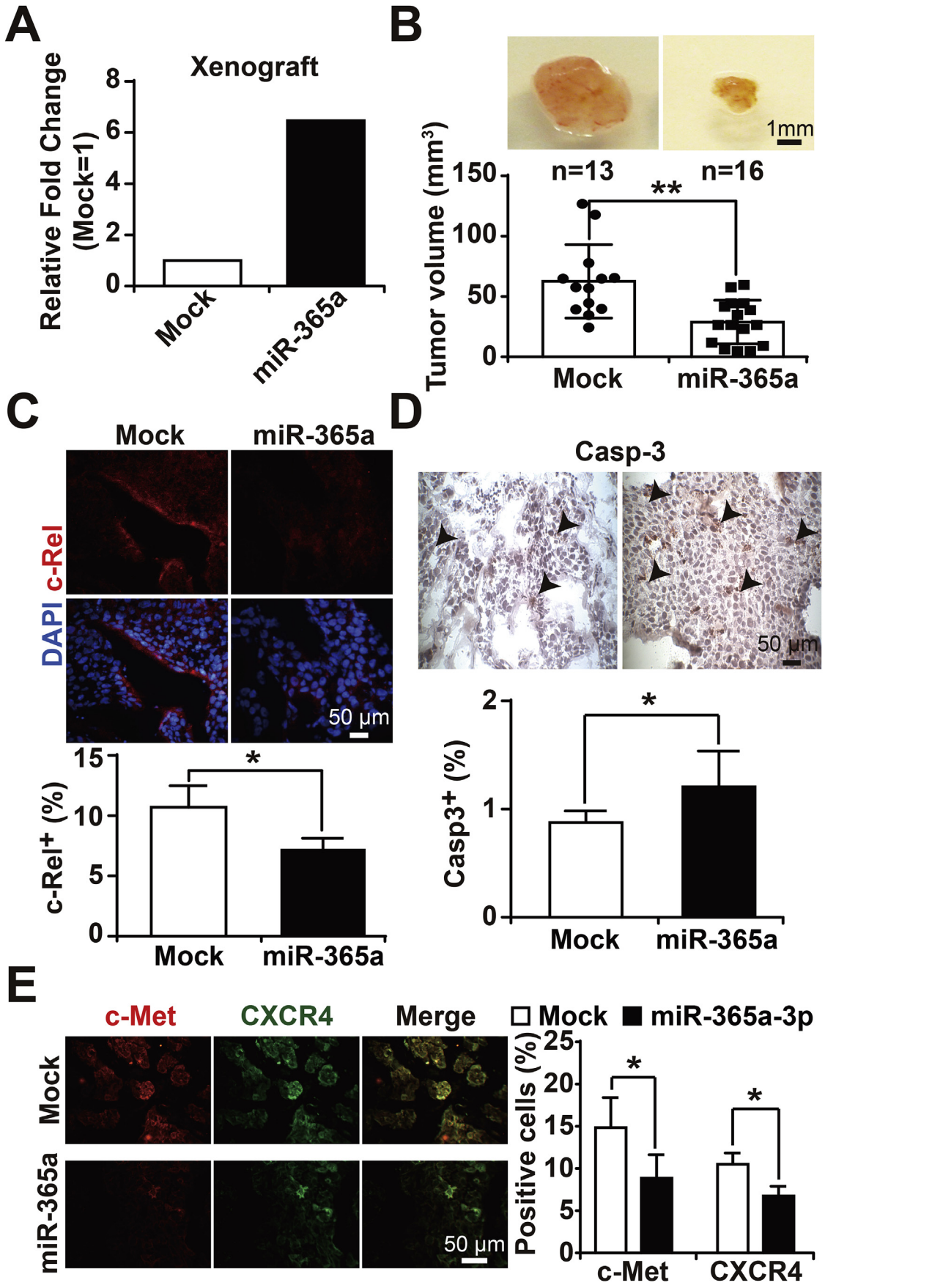

(caption on next page)

Fig. 4. miR-365a-3p reduces the volume of xenograft tumors. BxPC-3 cells were treated as indicated in Fig. 3A, and then cells (5×10^5) were seeded onto a CAM on day 9. Xenografts were collected and analyzed on day 18. (A) We used one mock xenograft and one miR-365a-3p-transfected xenograft for analysis. Total RNA was extracted from the xenografts, and the expression of miR-365a-3p was quantified by qPCR. (B) The tumor volumes are presented as black dots. The bar indicates the median tumor volume in each experimental group. Immunohistochemistry staining of the frozen tissue section was performed with (C) c-Rel, and the intensity of the immunofluorescence signal was quantified in ten vision fields with ImageJ. The means ± SD are shown. (D) Similarly, the expression of the apoptotic marker "cleaved fragment of activated caspase-3″ was detected, and positive, red to dark red signals are indicated by arrows. The numbers of positive cells were evaluated as described above. (E) Immunofluorescence staining of the pancreatic cancer stem cell marker c-Met and the metastasis and invasion marker CXCR4 were measured and evaluated as described above. (For interpretation of the references to color in this figure legend, the reader is referred to the Web version of this article.)

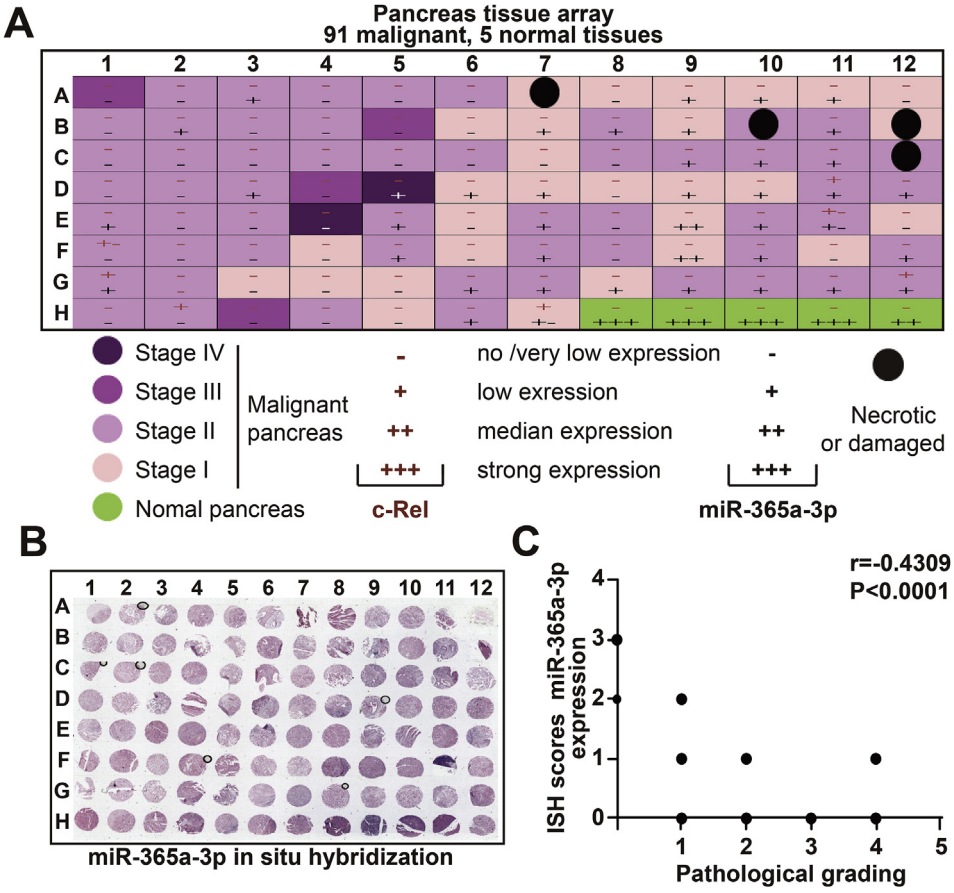

Fig. 5. Low miR-365a-3p expression correlates with malignancy. A paraffin-embedded tissue microarray slide containing 91 cases of pancreatic cancer and 5 normal pancreatic tissues was used. (A) A score of miR-365a-3p expression was evaluated by analyzing the expression patterns under 400 × magnification. The number of positive cells was quantified in 10 visual fields of each tissue. High (+++), medium (++), low (+), and absent (−) were used for scoring. (B) The expression of miR-365a-3p was detected by *in situ* hybridization, and positive cells appeared dark purple. A macroscopic photograph of the stained array is shown. Four tissues of the microarray were necrotic or damaged and thus were excluded from evaluation (thick black dot). (C) Scatter plot of miR365a-3p ISH scores in the pancreatic tissues, and the correlation with pathological grading is shown. $r = -0.4309$, $^{**}P < 0.001$. (For interpretation of the references to color in this figure legend, the reader is referred to the Web version of this article.)

much longer than those with high expression (n = 62).

Here, we also show that high levels of miR-365a-3p significantly inhibited cell viability, clonogenicity, migratory capacity and progression marker expression, as well as apoptosis induction. Our results are consistent with previous reports demonstrating that the overexpression of miR-365a-3p suppresses the binding activity of NF-κB and the percentage of induced apoptosis in PDA cells [6]. c-Rel is an anti-apoptotic player that regulates cellular signaling and function [31]. In line with our results, another study demonstrated that the siRNA-mediated knockdown of c-Rel markedly reduced the viability of PDA cells and induced apoptosis [27].

The chief challenge of miRNA delivery is to effectively deliver miRNA mimics to the target tumor tissue with competent dissemination of cargos into the tumor. For experimental studies, mice are the most common animal models used for miRNA delivery, but these models have high costs and administrative and ethical barriers. We used the fertilized chicken egg model as an excellent alternative, which has been evaluated in several of our recent studies [11,32–34], and we have improved the methodology for evaluating miRNA *in vivo* efficiency [19]. A major advantage of the chicken egg model is its natural immunodeficiency because immunocompetence in birds develops only after hatching. Xenografts are transplanted to the chorioallantoic membrane (CAM), usually between days 8–9 of development, when the blood vessel network is dense enough to support the growth of a tumor xenograft. Therefore, cells from different tissues and species can be transplanted as in immune-compromised mice. In addition, the CAM is noninnervated and allows painless tumor inoculation, growth and CAM injections. This feature is in contrast to the mouse system, where pain is induced by subcutaneous or orthotopic transplantation, subsequent tumor growth and injections. Additional advantages of CAM xenotransplantation compared to mice are faster tumor growth, which starts between 2 and 5 days after transplantation, and a well-developed histopathological morphology with tumor microenvironment, which resembles the microenvironment of primary patient tissue and the mouse xenograft. Additionally, the CAM model can be easily performed in any laboratory, as the method is inexpensive, and an animal application is not required until day 18 of embryonic chick development, when the xenografts have to be resected because the chick hatches on day 21. Thus, the chicken egg xenotransplantation model is well suited for short-term *in vivo* xenograft growth for up to 10 days.

Finally, we validated our concept of the miR-365a-3p-driven repression of c-Rel expression in a patient tissue array. Whereas the expression of miR-365a-3p was lower in malignant tissue, as expected, we had difficulties detecting c-Rel expression by immunohistochemistry because its expression was detectable in only 7 out of 91 malignant tissues. We do not know the potential reason for the almost absent

expression of c-Rel in patient tissue. However, there is complex cross-talk between different NF-κB subunits, and the loss of one NF-κB subunit usually leads to compensation by other NF-κB subunits [35–37]. Additionally, our surprising finding of almost absent c-Rel expression in malignant patient tissue matches the conflicting results regarding the function of NF-κB activity in the induction [38,39] and, in contrast, the inhibition [40,41] of apoptosis, as reported in a majority of publications. In agreement with a study on colitis-associated adenoma, animals lacking the c-Rel subunit were more susceptible to colitis-associated cancer than were wild-type mice, developing 3.5 times more colonic polyps per animal than in wild-type mice [24]. In contrast, a study of helicobacter-induced gastric carcinogenesis indicated that the loss of c-Rel alone did not drive gastric atrophy in wild-type mice [25]. Furthermore, a study with a melanoma mouse model found that tumor growth was drastically reduced in mice lacking c-Rel, and this effect was mediated via inhibiting regulatory T cells [42]. Consequently, the mechanisms through which c-Rel, as part of the NF-κB complex, orchestrates tumor progression or inhibition may vary between different cancer types, as different NF-κB subunits may compensate for each other [35–37].

In conclusion, we found an interesting function for miR-365a-3p in the inhibition of PDA progression, which was mediated by the inhibition of c-Rel in our experimental PDA models. Future studies are necessary to address whether the systemic application of miR-365a-3p in patients may inhibit NF-κB activity and thus improve the worse prognosis of patients suffering from PDA.

Ethical approval and consent to participate

Patient materials were obtained under the approval of the Ethics Committee of the University of Heidelberg after receiving written informed consent from the patients. The diagnoses were established by conventional clinical and histological criteria according to the World Health Organization (WHO). All surgical resections were indicated by the principles and practice of oncological therapy.

Consent for publication

All authors agree to the publication of this manuscript. This manuscript has not been published and is not under consideration for publication elsewhere.

Availability of supporting data

The datasets supporting the conclusions of this article are included within the article and its supplemental files and are thus available.

Conflicts of interest

The authors have no conflicts of interest to disclose regarding the publication of the present manuscript.

Author contributions

IH, LY: Concept and design.

LY, XX, CG: Development of methodology.

LY, XX, CG, JG, YY, SK, CS, YL: Acquisition of data.

LY, XX, CS, SK, LL, CS, NG, WG, IH: Analysis and interpretation of data.

LY, IH: Writing, review and/or revision of the manuscript.

Acknowledgments

We are grateful to C. DeLaTorre for technical advice and array analysis and S. Bauer and S. Faus for excellent technical assistance.

Appendix A. Supplementary data

Supplementary data to this article can be found online at https://doi.org/10.1016/j.canlet.2019.03.025.

Funding

This study was supported by the China Scholarship Council by a scholarship to L. Yin and by grants to I. Herr from the German Cancer Aid (Deutsche Krebshilfe 111299), the German Research Council (DFG HE 3186/15-1), Heidelberger Stiftung Chirurgie, Dietmar Hopp Stiftung, Klaus Tschira Stiftung and the Hanns A. Pielenz-Stiftung.

References

[1] R.L. Siegel, K.D. Miller, A. Jemal, Cancer statistics, Ca - Cancer J. Clin. 68 (2018) (2018) 7–30.
[2] J.P. Neoptolemos, J. Kleeff, P. Michl, E. Costello, W. Greenhalf, D.H. Palmer, Therapeutic developments in pancreatic cancer: current and future perspectives, Nat. Rev. Gastroenterol. Hepatol. 15 (2018) 333–348.
[3] S. Arora, A. Bhardwaj, S. Singh, S.K. Srivastava, S. McClellan, W.E. Grizzle, L.B. Owen, A.P. Singh, An undesired effect of chemotherapy: gemcitabine promotes pancreatic cancer cell invasiveness through upregulation of CXCR4, Cancer Res. 73 (2013).
[4] P.A. Baeuerle, D. Baltimore, Activation of DNA-binding activity in an apparently cytoplasmic precursor of the NF-kappa B transcription factor, Cell 53 (1988) 211–217.
[5] S. Grimm, P.A. Baeuerle, The inducible transcription factor NF-kappa B: structure-function relationship of its protein subunits, Biochem. J. 290 (Pt 2) (1993) 297–308.
[6] G. Kallifatidis, V. Rausch, B. Baumann, A. Apel, B.M. Beckermann, A. Groth, J. Mattern, Z. Li, A. Kolb, G. Moldenhauer, P. Altevogt, T. Wirth, J. Werner, P. Schemmer, M.W. Buchler, A.V. Salnikov, I. Herr, Sulforaphane targets pancreatic tumour-initiating cells by NF-kappaB-induced antiapoptotic signalling, Gut 58 (2009) 949–963.
[7] R.C. Lee, R.L. Feinbaum, V. Ambros, The C. elegans heterochronic gene lin-4 encodes small RNAs with antisense complementarity to lin-14, Cell 75 (1993) 843–854.
[8] A. Bhardwaj, S. Singh, A.P. Singh, MicroRNA-based cancer therapeutics: big hope from small RNAs, Mol. Cell. Pharmacol. 2 (2010) 213–219.
[9] M.V. Iorio, C.M. Croce, MicroRNA dysregulation in cancer: diagnostics, monitoring and therapeutics. A comprehensive review, EMBO Mol. Med. 4 (2012) 143–159.
[10] Y. Yin, L. Liu, Z. Zhao, L. Yin, N. Bauer, C.C. Nwaeburu, J. Gladkich, W. Gross, T. Hackert, C. Sticht, N. Gretz, O. Strobel, I. Herr, Simvastatin inhibits sonic hedgehog signaling and stemness features of pancreatic cancer, Cancer Lett. 426 (2018) 14–24.
[11] Z. Zhao, N. Bauer, E. Aleksandrowicz, L. Yin, J. Gladkich, W. Gross, J. Kaiser, T. Hackert, O. Strobel, I. Herr, Intraductal papillary mucinous neoplasm of the pancreas rapidly xenografts in chicken eggs and predicts aggressiveness, Int. J. Cancer 142 (2018) 1440–1452.
[12] P. Fan, Y. Zhang, L. Liu, Z. Zhao, Y. Yin, X. Xiao, N. Bauer, J. Gladkich, J. Mattern, C. Gao, P. Schemmer, W. Gross, I. Herr, Continuous exposure of pancreatic cancer cells to dietary bioactive agents does not induce drug resistance unlike chemotherapy, Cell Death Dis. 7 (2016) e2246.
[13] L. Liu, A.V. Salnikov, N. Bauer, E. Aleksandrowicz, S. Labsch, C. Nwaeburu, J. Mattern, J. Gladkich, P. Schemmer, J. Werner, I. Herr, Triptolide reverses hypoxia-induced EMT and stem-like features in pancreatic cancer by NF-kappa B downregulation, Int. J. Cancer 134 (2014) 2489–2503.
[14] A. Abukiwan, C.C. Nwaeburu, N. Bauer, Z. Zhao, L. Liu, J. Gladkich, W. Gross, A. Benner, O. Strobel, J. Fellenberg, I. Herr, Dexamethasone-induced inhibition of miR-132 via methylation promotes TGF-beta-driven progression of pancreatic cancer, Int. J. Oncol. 54 (2019) 53–64.
[15] P.S. Amponsah, P. Fan, N. Bauer, Z. Zhao, J. Gladkich, J. Fellenberg, I. Herr, microRNA-210 overexpression inhibits tumor growth and potentially reverses gemcitabine resistance in pancreatic cancer, Cancer Lett. 388 (2017) 107–117.
[16] M. Kanehisa, S. Goto, KEGG: kyoto encyclopedia of genes and genomes, Nucleic Acids Res. 28 (2000) 27–30.
[17] V. Agarwal, G.W. Bell, J.W. Nam, D.P. Bartel, Predicting effective microRNA target sites in mammalian mRNAs, Elife (2015) 4.
[18] L. Sevilla, A. Zaldumbide, P. Pognonec, K.E. Boulukos, Transcriptional regulation of the bcl-x gene encoding the anti-apoptotic Bcl-xL protein by Ets, Rel/NFkappaB, STAT and AP1 transcription factor families, Histol. Histopathol. 16 (2001) 595–601.
[19] C.C. Nwaeburu, E. Aleksandrowicz, N. Bauer, Z. Zhao, I. Herr, MicroRNA in Vivo Delivery to Human Pancreas Tumor Xenografts on Chicken Eggs, Protocol Exchange, (2017), https://doi.org/10.1038/nprot.2017.126.
[20] M. Xie, L. Ma, T. Xu, Y. Pan, Q. Wang, Y. Wei, Y. Shu, Potential regulatory roles of MicroRNAs and long noncoding RNAs in anticancer therapies, Mol. Ther. Nucleic Acids 13 (2018) 233–243.
[21] Y. Wang, S. Zhang, H. Bao, S. Mu, B. Zhang, H. Ma, S. Ma, MicroRNA-365 promotes lung carcinogenesis by downregulating the USP33/SLIT2/ROBO1 signalling

pathway, Cancer Cell Int. 18 (2018) 64.
[22] D.A. Calvopina, M.D. Chatfield, A. Weis, M.A. Coleman, M.A. Fernandez-Rojo, C. Noble, L.E. Ramm, D.H. Leung, P.J. Lewindon, G.A. Ramm, miRNA-seq Identifies a Serum miRNA Panel, Which Combined with APRI Can Detect and Monitor Liver Disease in Paediatric Cystic Fibrosis, Hepatology, (2018).
[23] J.E. Freedman, K. Tanriverdi, Defining miRNA targets: balancing simplicity with complexity, Circulation 127 (2013) 2075–2077.
[24] M.D. Burkitt, A.F. Hanedi, C.A. Duckworth, J.M. Williams, J.M. Tang, L.A. O'Reilly, T.L. Putoczki, S. Gerondakis, R. Dimaline, J.H. Caamano, D.M. Pritchard, NF-kappaB1, NF-kappaB2 and c-Rel differentially regulate susceptibility to colitis-associated adenoma development in C57BL/6 mice, J. Pathol. 236 (2015) 326–336.
[25] M.D. Burkitt, J.M. Williams, C.A. Duckworth, A. O'Hara, A. Hanedi, A. Varro, J.H. Caamano, D.M. Pritchard, Signaling mediated by the NF-kappaB sub-units NF-kappaB1, NF-kappaB2 and c-Rel differentially regulate Helicobacter felis-induced gastric carcinogenesis in C57BL/6 mice, Oncogene 32 (2013) 5563–5573.
[26] P.C. Cogswell, D.C. Guttridge, W.K. Funkhouser, A.S. Baldwin Jr., Selective activation of NF-kappa B subunits in human breast cancer: potential roles for NF-kappa B2/p52 and for Bcl-3, Oncogene 19 (2000) 1123–1131.
[27] C. Geismann, F. Grohmann, S. Sebens, G. Wirths, A. Dreher, R. Hasler, P. Rosenstiel, C. Hauser, J.H. Egberts, A. Trauzold, G. Schneider, B. Sipos, S. Zeissig, S. Schreiber, H. Schafer, A. Arlt, c-Rel is a critical mediator of NF-kappaB-dependent TRAIL resistance of pancreatic cancer cells, Cell Death Dis. 5 (2014) e1455.
[28] H. Lu, X. Yang, P. Duggal, C.T. Allen, B. Yan, J. Cohen, L. Nottingham, R.A. Romano, S. Sinha, K.E. King, W.C. Weinberg, Z. Chen, C. Van Waes, TNF-alpha promotes c-REL/DeltaNp63alpha interaction and TAp73 dissociation from key genes that mediate growth arrest and apoptosis in head and neck cancer, Cancer Res. 71 (2011) 6867–6877.
[29] J.E. Hunter, J. Leslie, N.D. Perkins, c-Rel and its many roles in cancer: an old story with new twists, Br. J. Canc. 114 (2016) 1–6.
[30] L. Li, Z.Y. Xu-Monette, C.Y. Ok, A. Tzankov, G.C. Manyam, R. Sun, C. Visco, M. Zhang, S. Montes-Moreno, K. Dybkaer, A. Chiu, A. Orazi, Y. Zu, G. Bhagat, K.L. Richards, E.D. Hsi, W.W. Choi, J.H. van Krieken, J. Huh, M. Ponzoni, A.J. Ferreri, M.B. Moller, J. Wang, B.M. Parsons, J.N. Winter, M.A. Piris, L.V. Pham, L.J. Medeiros, K.H. Young, Prognostic impact of c-Rel nuclear expression and REL amplification and crosstalk between c-Rel and the p53 pathway in diffuse large B-cell lymphoma, Oncotarget 6 (2015) 23157–23180.
[31] T.D. Gilmore, S. Gerondakis, The c-rel transcription factor in development and disease, Genes Cancer 2 (2011) 695–711.
[32] L. Liu, A.V. Salnikov, N. Bauer, E. Aleksandrowicz, S. Labsch, C. Nwaeburu, J. Mattern, J. Gladkich, P. Schemmer, J. Werner, I. Herr, Triptolide reverses hypoxia-induced epithelial-mesenchymal transition and stem-like features in pancreatic cancer by NF-kappaB downregulation, Int. J. Cancer 134 (2014) 2489–2503.
[33] E. Aleksandrowicz, I. Herr, Ethical euthanasia and short-term anesthesia of the chick embryo, ALTEX 32 (2015) 143–147.
[34] L. Liu, E. Aleksandrowicz, F. Schonsiegel, D. Groner, N. Bauer, C.C. Nwaeburu, Z. Zhao, J. Gladkich, T. Hoppe-Tichy, E. Yefenof, T. Hackert, O. Strobel, I. Herr, Dexamethasone mediates pancreatic cancer progression by glucocorticoid receptor, TGFbeta and JNK/AP-1, Cell Death Dis. 8 (2017) e3064.
[35] M. Grossmann, D. Metcalf, J. Merryfull, A. Beg, D. Baltimore, S. Gerondakis, The combined absence of the transcription factors Rel and RelA leads to multiple hemopoietic cell defects, Proc. Natl. Acad. Sci. U. S. A. 96 (1999) 11848–11853.
[36] J. Sun, P. Huang, J. Liang, J. Li, M. Shen, X. She, Y. Feng, X. Luo, T. Liu, X. Sun, Cooperation of Rel family members in regulating Abeta1-40-mediated pro-inflammatory cytokine secretion by retinal pigment epithelial cells, Cell Death Dis. 8 (2017) e3115.
[37] N.D. Perkins, The diverse and complex roles of NF-kappaB subunits in cancer, Nat. Rev. Canc. 12 (2012) 121–132.
[38] C. Jennewein, S. Karl, B. Baumann, O. Micheau, K.M. Debatin, S. Fulda, Identification of a novel pro-apoptotic role of NF-kappaB in the regulation of TRAIL- and CD95-mediated apoptosis of glioblastoma cells, Oncogene 31 (2012) 1468–1474.
[39] B. Kaltschmidt, C. Kaltschmidt, T.G. Hofmann, S.P. Hehner, W. Droge, M.L. Schmitz, The pro- or anti-apoptotic function of NF-kappaB is determined by the nature of the apoptotic stimulus, Eur. J. Biochem. 267 (2000) 3828–3835.
[40] M.M. Chaturvedi, B. Sung, V.R. Yadav, R. Kannappan, B.B. Aggarwal, NF-kappaB addiction and its role in cancer: 'one size does not fit all', Oncogene 30 (2011) 1615–1630.
[41] R. Hamacher, R.M. Schmid, D. Saur, G. Schneider, Apoptotic pathways in pancreatic ductal adenocarcinoma, Mol. Canc. 7 (2008) 64.
[42] Y. Grinberg-Bleyer, H. Oh, A. Desrichard, D.M. Bhatt, R. Caron, T.A. Chan, R.M. Schmid, U. Klein, M.S. Hayden, S. Ghosh, NF-kappaB c-rel is crucial for the regulatory T cell immune checkpoint in cancer, Cell 170 (2017) 1096–1108 e1013.